Substate Excitation of 2^+ States Produced by Inelastic Scattering of Protons on ^{12}C, ^{54}Fe, and ^{58}Ni†*

J. R. Tesmer‡ and F. H. Schmidt
Department of Physics, University of Washington, Seattle, Washington 98195
(Received 19 October 1971)

A combined analysis of absolute in-plane and z-axis (spin-flip) p-γ angular correlation measurements for 0^+-2^+-0^+ transitions leads to various combinations of substate cross sections, populations, and phase angles. These quantities are compared with predictions based on reaction-mechanism theories. The test is very stringent. Measurements and analyses have been carried out for $^{12}C(p,p'\gamma)^{12}C^*(4.44\ \text{MeV})$ and $^{58}Ni(p,p'\gamma)^{58}Ni^*(1.45\ \text{MeV})$ at $E_p = 20$ MeV, and for $^{54}Fe(p,p'\gamma)^{54}Fe^*(1.41\ \text{MeV})$ at $E_p = 19.6$ MeV.

Each of the three nuclei studied exhibits the following qualitative features: (1) The total inelastic cross sections have a less pronounced structure than do the individual substate cross sections. (2) The $M=0$ cross section is the most diffractionlike; the oscillations are out of phase with respect to the oscillations of the elastic cross section. (3) The sum of the $M=+2$ and $M=-2$ cross sections also are diffractionlike, but are not in phase with the $M=0$.

Detailed comparisons with collective-model distorted-wave Born-approximation predictions are, on the whole, quite good for ^{58}Ni and ^{54}Fe, especially when the full Thomas form for the spin-dependent perturbation potential is used. The isotropic term in the in-plane angular-correlation function is particularly sensitive to the form and strength of the spin-orbit coupling potential. For ^{54}Fe the predictions are further improved when the strength of the spin-dependent perturbation potential is increased by setting the spin-dependent deformation equal to twice the central-potential deformation.

I. INTRODUCTION

The process of inelastic proton scattering to 2^+ states from 0^+ ground states leaves a nucleus in one or another of five different "magnetic" substates. Various combinations of parameters which describe these substates, as for example, the sum of the $M=+2$ and -2 amplitudes, can be determined by appropriate combined analysis of absolute proton-γ angular-correlation measurements made in the reaction plane, and perpendicular to the reaction plane. Each such combination is then comparable to reaction theory. The method thus provides a more stringent test of theoretical descriptions of the scattering process than does a measurement of the inelastic cross section alone.

The general method was first applied for the ^{12}C nucleus at 10.5-MeV incident proton energy for a very limited number of proton scattering angles.[1] In this paper we present the results of similar combined measurements over a large range of proton scattering angles for ^{12}C and ^{58}Ni at 20 MeV, and for ^{54}Fe at 19.6 MeV.[2] A preliminary report of some of our work was published in abstract form[3]; a discussion of the special significance of the parameter A in the correlation function appears in one of our previous papers.[4]

The z-axis (or spin-flip) data for ^{12}C and ^{58}Ni were published previously.[5,6] We have performed similar measurements for ^{54}Fe; Hendrie *et al.*[7] have also measured the spin-flip for ^{54}Fe at 19.6 MeV.

In Sec. II we review the theory of the method. Our experimental methods and results are described in Secs. III and IV, respectively. Section V contains comparisons with calculations based on the collective model in the distorted-wave Born approximation (DWBA).

II. THEORY OF THE MEASUREMENT

A. General Correlation Function

A proton-γ angular (or directional) correlation is defined as the probability that an inelastically scattered proton (exciting the 2^+ state) will be scattered at angles θ_p and ϕ_p and the deexcitation γ ray will be emitted at angles θ_γ and ϕ_γ. The form for this type of correlation has been derived by several authors.[8,9] In general, it can be written as

$$W(\theta_p, \phi_p; \theta_\gamma, \phi_\gamma) = \mathrm{Tr}\rho\eta\,, \tag{1}$$

where ρ and η are called statistical or density matrices. The matrix ρ describes the excitation of the 2^+ state by proton scattering and is a function only of the scattered proton coordinates θ_p and ϕ_p. Similarly, η describes the deexcitation of the state by γ-ray emission and depends only on the γ-ray coordinates θ_γ and ϕ_γ. In particular,

an element of ρ is written as

$$\rho_{MM'} = \sum_{\mu_i \mu_f} T(\mu_i \mu_f, M) T^*(\mu_i \mu_f, M'), \tag{2}$$

where $T(\mu_i \mu_f, M)$ is the amplitude for exciting the M^{th} substate ($M = 0, \pm 1, \pm 2$) with an incident proton with spin projection μ_i and the scattered proton with spin projection μ_f. The amplitudes are normalized such that $\mathrm{Tr}\rho = 1$.

The matrix elements of η are

$$\eta_{M'M} = \vec{X}^*_{2M'} \cdot \vec{X}_{2M}, \tag{3}$$

where the $\vec{X}$'s are vector spherical harmonics. The correlation function is normalized so that

$$\int W d\Omega_\gamma = 1. \tag{4}$$

The measurement of the correlation function W, therefore, determines ρ, since η is well known. This determination is completely independent of any nuclear model.

B. Coordinate System

An appropriate choice of coordinate system greatly simplifies the interpretation of the results of the measurements. If the z axis is chosen perpendicular to the reaction plane, restrictions are placed on the excitation of certain substates. These restrictions come from a reaction-plane symmetry theorem given by Bohr.[10] Application of this theorem to the excitation of a 2^+ state of an even-even nucleus by protons leads to the following restrictions: if $\Delta\mu = \mu_i - \mu_f = \pm 1$, then $M = \pm 1$, and if $\Delta\mu = 0$, then $M = 0$, or ± 2. We see that the protons which flip their spins during the interaction ($\Delta\mu = \pm 1$) will have excited only the $M = \pm 1$ substates. Hence, in the absence of spin flip only the $M = 0, \pm 2$ substates will have been excited.

It is clear that there are two incoherent processes – one for $\Delta\mu = \pm 1$ and one for $\Delta\mu = 0$. These processes do not interfere, hence, interference terms between them do not appear in the correlation function. This fact limits the terms in the correlation function to those for which $M + M'$ is even.

We have defined the z axis in the direction $\hat{K}_{\text{inc}} \times \hat{K}_f$ where $\hat{K}_{\text{inc}}$ and $\hat{K}_f$ are unit vectors along the incident beam direction and the direction of the scattered proton, respectively. The x axis is along the beam direction $\hat{K}_{\text{inc}}$.

C. Correlation Functions

The in-plane correlation function may be written as

$$W(\theta_p = \tfrac{1}{2}\pi, \phi_p; \theta_\gamma = \tfrac{1}{2}\pi, \phi_\gamma) = \frac{5}{16\pi}[D - E_1 \cos 2(\phi_\gamma - \epsilon_1) - E_2 \cos 4(\phi_\gamma - \epsilon_2)], \tag{5}$$

where

$$\begin{aligned} D &= \sum_m (\rho_{mm} + \rho_{-m-m}), \\ E_m &= 2|\rho_{m,-m}|, \\ \epsilon_m &= -(\arg \rho_{m,-m})/2m, \end{aligned} \tag{6}$$

for $m = 1, 2$ only. A more detailed description of these terms, written in terms of amplitudes, has been given in Ref. 1.

For a given proton scattering angle (ϕ_p) the five parameters D, $E_{1,2}$, and $\epsilon_{1,2}$ can be determined experimentally. Another, and more common form for Eq. (5) is

$$W(\theta_p = \tfrac{1}{2}\pi, \phi_p; \theta_\gamma = \tfrac{1}{2}\pi, \phi_\gamma) = \frac{5}{16\pi}[A + B \sin^2 2(\phi_\gamma - \epsilon_2) + C \sin^2(\phi_\gamma - \epsilon_1)]. \tag{7}$$

This is analogous to the form used in most α-γ correlation studies with the addition of the spin-flip-dependent term, $C \sin^2(\phi_\gamma - \epsilon_1)$. The roles of B and C have been reversed from those used in previous papers.[1,4] The above coefficients are related to those of Eq. (5) by

$$A = D - E_1 - E_2, \quad B = 2E_2, \quad C = 2E_1. \tag{8}$$

For α-γ correlations A is equal to the nuclear polarization. For p-γ correlations, however, A is complicated by the spin of the proton. In particular, A can be written in terms of the amplitudes defined in Eq. (2) as

$$\begin{aligned} A = \sum_m \sum_{\mu_i, \mu_f} [\,|T(\mu_i \mu_f, m)| - |T(\mu_i \mu_f, -m)|\,]^2 \\ - 2 \sum_m \sum_{\substack{\mu_i, \mu_f; \mu_i', \mu_f' \\ \mu_i \neq \mu_i', \mu_f \neq \mu_f'}} T(\mu_i \mu_f, m) T^*(\mu_i' \mu_f, -m) \\ \times T^*(\mu_i' \mu_f', m) T(\mu_i' \mu_f', -m), \end{aligned} \tag{9}$$

for $m = 1, 2$ only. The restrictions placed on the amplitudes by the Bohr theorem (see Sec. II B) must also be observed. The first term is the nuclear polarization. The second term, however, is probably nonzero and prevents A from being analogous to the expression for α-particle scattering.

Because of our choice of coordinate system the γ detector is positioned on the negative ($-\phi_\gamma$) side of the beam. Therefore, we have defined the phase angles to be the angle at which the first minimum occurs, on the negative side of the beam, of each of the two terms of the correlation function.

The z-axis correlation is given by

$$W(\theta_p = \tfrac{1}{2}\pi, \phi_p; \theta_\gamma = 0) = \frac{5}{8\pi}[\rho_{11} + \rho_{-1-1}]. \tag{10}$$

D. Combined Correlation

We define the following combinations of the density matrix elements:

$$S_0 = \rho_{00}\,, \quad S_1 = \rho_{11} + \rho_{-1-1}\,, \quad S_2 = \rho_{22} + \rho_{-2-2}\,, \tag{11}$$

where the S_M's are the probabilities for exciting the $|M|^{\text{th}}$ substates with an unpolarized incident beam. The substate probabilities (or populations) are normalized so that

$$S_0 + S_1 + S_2 = 1\,. \tag{12}$$

The constant term D of Eq. (5), in the in-plane correlation can be rewritten as

$$D = 1 - S_0\,. \tag{13}$$

The z-axis correlation measures S_1; hence, with Eq. (13) and the normalization condition all of the S_M's are determined. The substate cross sections are found from the S_M's by simply multiplying the inelastic cross section by the S_M's at any given proton angle.

III. EXPERIMENTAL METHOD

A. Accelerator, Scattering Chamber, and Proton Detectors

The proton beam used in these experiments was produced by the University of Washington three-stage tandem Van de Graaff accelerator.[11] The energy resolution of the beam was from 2–5 keV.

The experiment was performed in a 60-in.-diam scattering chamber; all detectors were located within its vacuum. Details of the scattering chamber and beam focusing mechanisms have been described in Ref. 6.

The scattered protons were detected with an array of five 2.95-mm-thick lithium-drifted silicon detectors spaced 10° apart. The defining apertures subtended an in-plane full angle of 2° at 15.22 cm from the target center. The out-of-plane full angle was 6°. The solid angle subtended at this distance was $\sim 3.59 \times 10^{-3}$ sr. Antiscatter baffles were used in front of the defining apertures to limit the detector's view to a spot ~6.3 mm wide in the reaction plane at target center. The actual beam spot was <4 mm in diameter.

The detector array was operated at liquid-nitrogen temperatures in order to produce better timing by reducing noise and decreasing the charge collection time. The liquid-nitrogen cooling system has been described by Hayward.[12]

B. γ Detectors

Two γ detectors were employed: an RCA 7046 photomultiplier coupled to a 10-cm-diam by 10-cm-long NaI(Tl) crystal was used for the ^{12}C and ^{58}Ni targets, and an RCA 4522 coupled to a 12.7-cm-diam by 10-cm-long NaI(Tl) crystal was used for the ^{54}Fe target. The latter detector has improved energy resolution, smaller gain shifts due to counting rates, and a faster-rising anode signal.

Each γ detector was equipped with two interchangeable lead shields: one for the in-plane measurements and one for the z-axis measurements. The in-plane shields had rectangular apertures with half angles 5° high by 5.5° wide. The z-axis shields had circular apertures with 11° half angles. A lead absorber ~3 mm thick was placed between the target and crystal to reduce the flux of low-energy γ rays.

Each γ-detector shield assembly was calibrated so that the product of its absolute efficiency and effective solid angle was known as a function of the fraction of the spectrum for a monoenergetic γ ray above a given energy. The methods for calibration have been discussed by Hayward[12] and Mitchell.[13]

C. Targets

The ^{12}C target was a self-supporting natural carbon foil. The ^{54}Fe and ^{58}Ni targets were isotopically enriched self-supporting foils. The materials for the ^{54}Fe and ^{58}Ni targets were 1.0 mg/cm^2 thick. The ^{12}C target was ~0.7 mg/cm^2.

D. Electronics

Each of the five proton detectors and the γ detector produced a fast-rising timing signal and an integrated signal proportional to the energy lost in the detector. Fast-rising timing signals were obtained from the proton detectors with direct-coupled time pick-off preamplifiers with circuitry similar to that described by Sherman, Roddick, and Metz.[14] The saturated anode pulse from the photomultiplier was used for the γ-ray timing signal. The "fast" coincidences were determined with two time-to-amplitude converters – one for the two forward-angle proton detectors and one for the three remaining detectors.

Five fast-slow coincident systems were used. A true fast-coincidence event between a proton and γ ray has to be associated with a γ ray with energy above some chosen lower energy limit and with an inelastically scattered proton from the first 2^+ state. The coincidence resolving time of the systems, as represented by the full width at background level, was 10–15 nsec. The full width at half maximum was ~2 nsec. The five coincident time spectra, as well as the five proton spectra gated by single-channel analyzers with windows set to only allow protons which excited the 2^+ state,

were stored, on line, in an SDS 930 computer. In addition, the γ spectrum gated by a low-level discriminator, and the spectrum of a monitor detector (additional detector used to monitor the target thickness) were both stored in Nuclear Data analyzers. At the end of each data collection run (~1 h) each of the memories of the Nuclear Data analyzers were read into the SDS 930 computer. All of the collected spectra were then printed and plotted.

The on-line collection program[15] also monitored the values of the correlation parameters and their errors, as well as other critical quantities such as analog-to-digital-converter dead times, beam energy, etc.

E. Data Analysis

The measured value of the correlation, $\overline{W}$, is given by

$$\overline{W} = T/PF \,, \tag{14}$$

where T is the number of true coincident events in the gated time spectrum, and P is the number of inelastic protons observed in the inelastic proton peak. Both these quantities are corrected for electronic dead times. The quantity F is the efficiency–solid-angle factor for the γ detector.

The uncertainty in $\overline{W}$ is found by the usual combination of the uncertainties of T, P, and F. The uncertainty in F derives primarily from the calibration measurement and is ~±2%. The number of true coincident events, T, and its uncertainty, are determined from the coincident time spectra by the method given by Hayward and Schmidt.[16]

The measured z-axis correlation is related to the substate populations by

$$\overline{W}_z = \frac{5}{8\pi}(\overline{D}S_0 + \overline{G}S_1 + \overline{F}S_2) \,, \tag{15}$$

where $\overline{D}$, $\overline{G}$, and $\overline{F}$ are solid-angle correction factors. Calculations for these are discussed in the Appendix. For point detectors $\overline{D} = \overline{F} = 0$, $\overline{G} = 1$.

Similarly, the in-plane measurement is related to the in-plane parameters by

$$\overline{W}_{\text{in}}(\phi_\gamma) = \frac{5}{16\pi}[D' - C_1E_1\cos 2(\phi_\gamma - \epsilon_1) - C_2E_2\cos 4(\phi_\gamma - \epsilon_2)] \,, \tag{16}$$

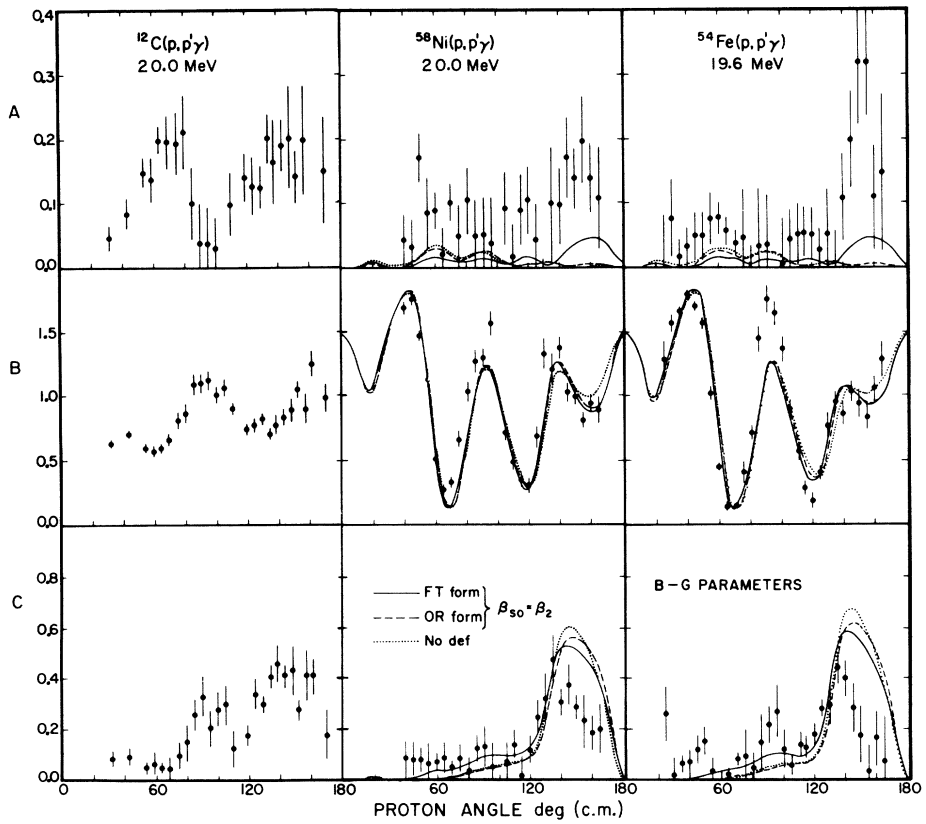

FIG. 1. In-plane correlation parameters A, B, and C. The curves are DWBA predictions with various forms of the spin-dependent interaction potential.

where

$$D' = 1 - \bar{A}S_0 - \bar{B}S_1 - \bar{C}S_2 . \quad (17)$$

Here again $\bar{A}$, $\bar{B}$, $\bar{C}$, C_1, and C_2 are detector solid-angle correction factors and are discussed in the Appendix. For point detector geometries, $\bar{A} = C_1 = C_2 = 1$, and $\bar{B} = \bar{C} = 0$.

The number of γ detector angles used in determining $\bar{W}_{in}$ varied from 7 to 16. The measured correlation function was fitted by the method of least squares to a linearized form of Eq. (16). The least-squares fit was performed by matrix inversion.[17] The linearized parameters were then combined to yield the "original" correlation parameters of Eq. (16). The uncertainties and coefficients of correlation of the linear parameters were taken from the inverse matrix from the least-squares fit and were used to calculate the uncertainties in the original correlation parameters.

Since the correlation measurements we report here are absolute, the z-axis and in-plane results may be combined to yield the substate populations and cross sections. From the in-plane correlation we take the expression for D' and combine it with $\bar{W}_z$ and the normalization condition. This is done by solving the three simultaneous equations

$$\begin{aligned} &\bar{A}S_0 + \bar{B}S_1 + \bar{C}S_2 = 1 - D' , \\ &\bar{D}S_0 + \bar{G}S_1 + \bar{F}S_2 = \tfrac{8}{5}\pi\bar{W}_z , \\ &S_0 + S_1 + S_2 = 1 . \end{aligned} \quad (18)$$

The simultaneous solution to these equations gives the substate populations S_0, S_1, and S_2. The substate cross sections are calculated by multiplying the substate populations by the inelastic cross section, i.e.,

$$\sigma_i = S_i(d\sigma_{2^+}/d\Omega) , \quad i = 0, 1, 2 . \quad (19)$$

IV. RESULTS

A. In-Plane Correlation Parameters

We have chosen the parameters A, B, and C to represent the in-plane correlation rather than D, E_1, and E_2. These parameters, particularly parameter A, give special insight into the scattering process. The relationships between these two sets of parameters are given in Eq. (8).

The experimentally determined in-plane correlation parameters A, B, and C are shown in Fig. 1 for all three nuclei. In general, the features of these parameters are similar for all three nuclei.

Parameter A is small for all the nuclei – the maximum value is <0.4. The most noticeable feature is the backward-angle peak (~150°). A forward-angle (~70°) peak is also evident for ^{12}C.

Parameter B is related to the amplitude of the $M = \pm 2$ substates as is seen from Eqs. (6) and (8). The shape of this coefficient is similar to that of S_2.

Parameter C is related to the amplitude of the $M = \pm 1$ substates. It is, therefore, associated with spin flip. In all cases C has the same shape as the spin-flip probability, S_1.

The phase angles ϵ_1 and ϵ_2 are shown in Fig. 2. The phase angle ϵ_1 is the much more difficult of

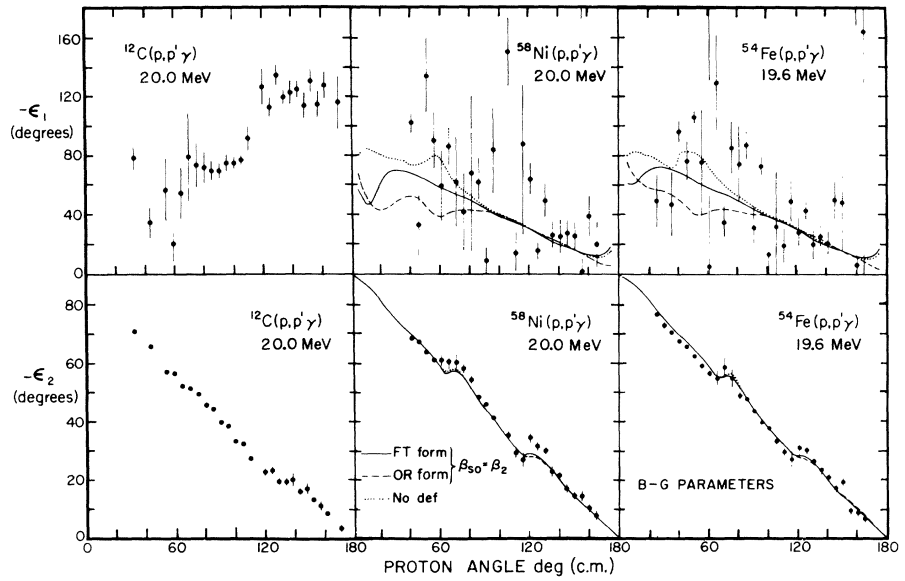

FIG. 2. In-plane correlation phase angles. The curves are DWBA predictions with various forms of the spin-dependent interaction potential.

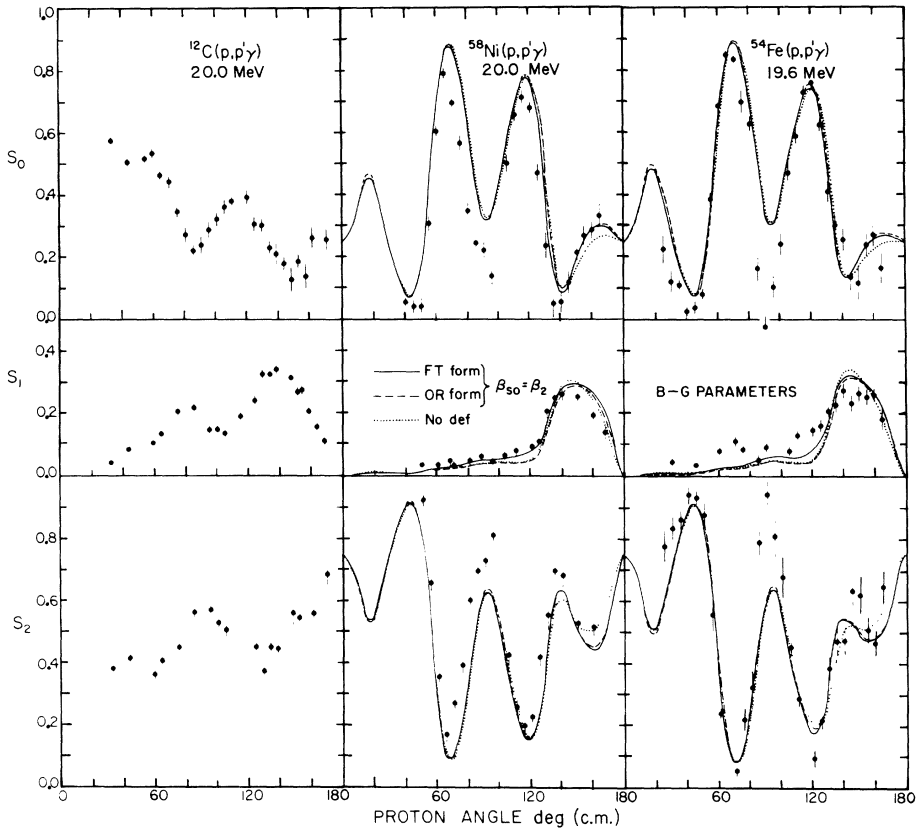

FIG. 3. Substate populations S_0, S_1, and S_2. The curves are DWBA predictions with various forms of the spin-dependent interaction potential.

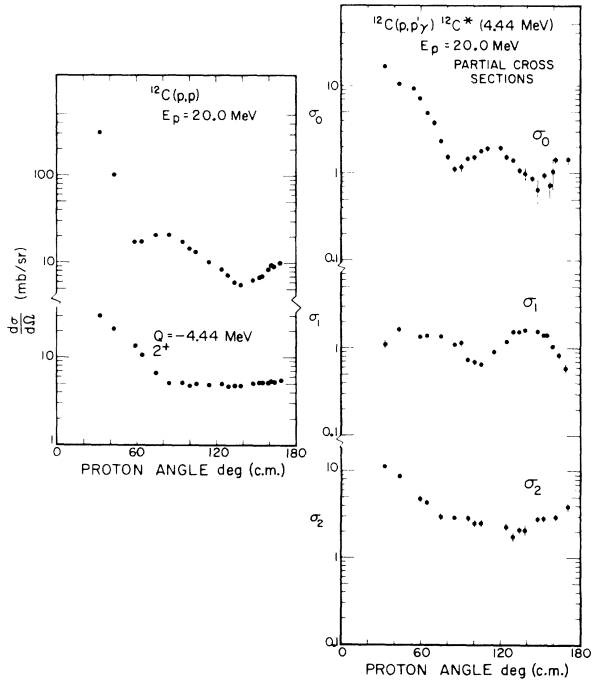

FIG. 4. Elastic, inelastic, and substate cross sections for ^{12}C.

the two to determine (as reflected by its uncertanties), since the coefficient C is usually very small.

For all three nuclei, ϵ_2 is almost linear and, in fact, is almost identical to the nuclear adiabatic recoil angle.

The phase angle ϵ_1 is certainly not adiabatic in the case of ^{12}C. The uncertainties are rather large for both ^{58}Ni and ^{54}Fe so that no conclusions about the adiabaticity of ϵ_1 can be drawn.

B. Substate Populations and Cross Sections

The substate populations are shown in Fig. 3.

The substate population S_0 exhibits maxima at proton angles corresponding to minima in the elastic cross sections for all nuclei studied. However, S_0 does not oscillate as strongly for ^{12}C as for ^{58}Ni or ^{54}Fe.

The spin-flip probabilities S_1 are relatively small and have large peaks at proton scattering angles of ~140°. In addition, ^{12}C and ^{54}Fe have smaller forward-angle peaks.

Because of the normalization condition and because S_1 is relatively small, S_2 oscillates out of

phase with S_0. For ^{12}C the oscillations are quite weak.

The elastic, inelastic, and substate cross sections are shown in Figs. 4 through 6. In all cases the inelastic cross section shows weak oscillations. The substate cross sections, on the other hand, oscillate strongly and exhibit features of diffraction scattering. The substate cross section σ_0 oscillates out of phase with the elastic cross section. This behavior is reminiscent of the Blair phase rule for the inelastic scattering of α particles.[18]

V. THEORETICAL INTERPRETATION OF THE RESULTS

A. Adiabatic Approximation

One of the simplifying assumptions that can be made in the theoretical predictions is the adiabatic approximation. This approximation assumes that: (1) The internal motion of the target nucleus is "frozen" during the collision[19] and (2) the initial and final momenta of the projectile are of equal magnitude.

For spin-zero projectiles Blair and Wilets[20] have shown that in the adiabatic approximation: (1) Parameter A is zero and (2) the phase angle ϵ_2 lies along the adiabatic nuclear recoil angle. Similarly, for spin-$\frac{1}{2}$ projectiles Sherif[21] has shown that both the phase angles ϵ_1 and ϵ_2 lie along the adiabatic recoil angle. In this case, however, parameter A will not necessarily be zero owing to the effects of the spin-flip-dependent amplitudes.

An examination of our results shows: (1) ϵ_2 follows the adiabatic angle very closely for all three nuclei (there are, however, two inflections); (2) parameter A for ^{54}Fe and ^{58}Ni is near zero over most of the angular range; and (3) ϵ_1 for both ^{58}Ni and ^{54}Fe, although not very accurately determined, has an adiabatic trend. These results clearly support the over-all features of the adiabatic approximation. On the other hand, ^{12}C is contradictory, since ϵ_1 is distinctly nonadiabatic. This points out the different nature of the spin-dependent interaction for ^{12}C. A more detailed examination of the implications of adiabaticity, especially for parameter A, is given in Ref. 4.

B. Collective Model

The collective model with the DWBA is used to predict the experimental results (the adiabatic approximation is not used). Predictions for ^{12}C are not given, since the model is not valid for nuclei with small numbers of nucleons or strongly excited 2^+ states.

A standard optical potential is used for the predictions. It is identical to that given by Becchetti and Greenlees[22] and by other authors.[6,23] The standard optical parameters (B-G) used are given

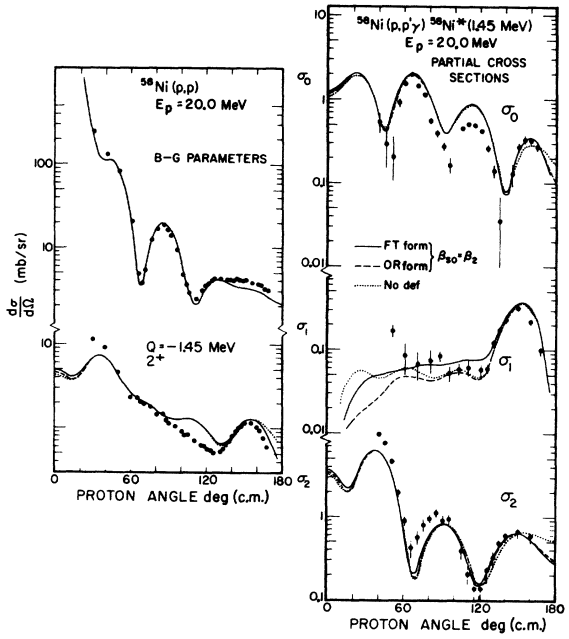

FIG. 5. Elastic, inelastic, and substate cross sections for ^{58}Ni. The curves are DWBA predictions with various forms of the spin-dependent interaction potential.

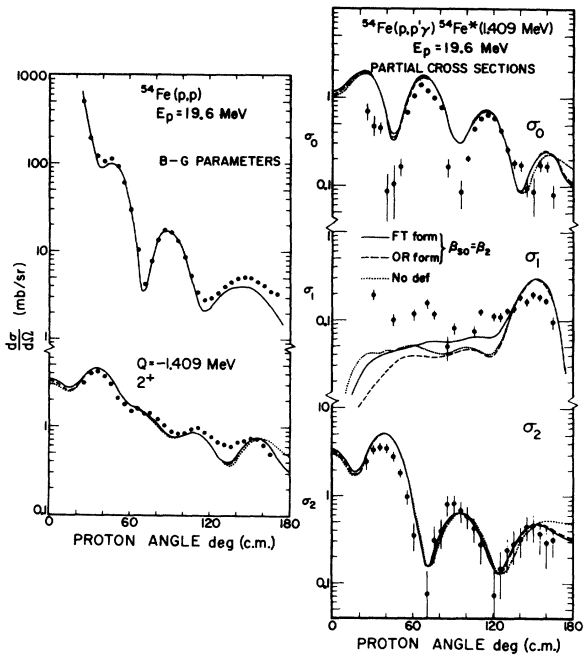

FIG. 6. Elastic, inelastic, and substate cross sections for ^{54}Fe. The curves are DWBA predictions with various forms of the spin-dependent interaction potential.

TABLE I. Standard optical-model parameters.

Nucleus	V_R	W	W_S	V_{so}	r_R	r_I	r_{so}	r_C	a_R	a_I	a_{so}	β_2	Incident energy (MeV)
^{58}Ni	51.3	1.7	7.2	6.2	1.17	1.32	1.01	1.25	0.75	0.53	0.75	0.21	20.0
^{54}Fe	51.4	1.6	7.3	6.2	1.17	1.32	1.01	1.25	0.75	0.54	0.75	0.17	19.6

in Table I. These parameters are the result of fitting the elastic cross section and polarization data of a large number of nuclei and are, therefore, very general in nature. Other sets of parameters were tried but the results were found not to differ greatly from those with the parameters of Table I.

The collective-model interaction is derived from the optical model by deforming the nuclear radius:

$$R \to R + \alpha(\hat{r}) . \tag{20}$$

The optical potential $U(r, R)$ can then be expanded in a Taylor's series to first order in $\alpha(\hat{r})$,

$$U(r, R + \alpha(\hat{r})) = U(r, R) + \Delta U(r, R, \alpha(\hat{r})) , \tag{21}$$

where ΔU is the perturbation (or interaction) potential for forming the excited state and is proportional to $\alpha(\hat{r})$.

The general form of the transition amplitude to such an excited state has been given by a number of authors. We use the notation of Sherif.[23] The DWBA expression for the transition amplitude is

$$T_{i\to f} = \langle \chi^{(-)}(\hat{K}_f, \hat{r}) | \langle IM | \Delta U | 00 \rangle | \chi^{(+)}(\hat{K}_{\rm inc}, \hat{r}) \rangle , \tag{22}$$

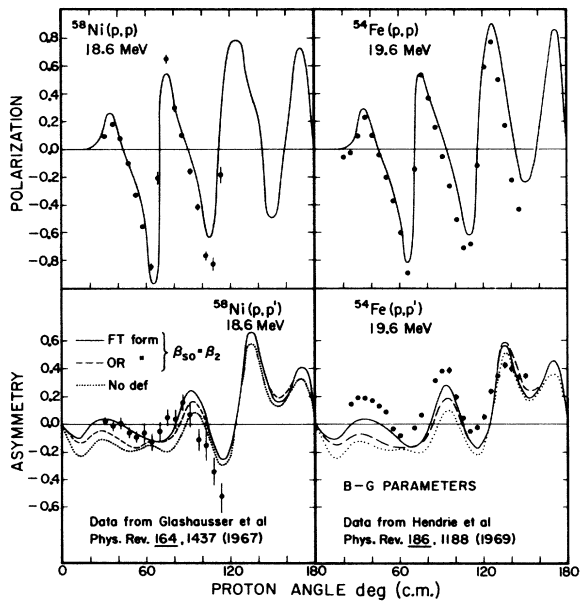

FIG. 7. Polarization and inelastic asymmetry data for ^{58}Ni and ^{54}Fe. The curves are DWBA predictions with various forms of the spin-dependent interaction potential.

where $|IM\rangle$ and $|00\rangle$ represent the excited and ground-state wave functions of the nucleus, respectively, and $\chi^{(-)}$ and $\chi^{(+)}$ are the outgoing and incoming asymptotic forms of the eigenfunctions for elastic scattering, respectively. The χ's are also functions of the projectile's spin.

The dependence of ΔU on the nuclear coordinates is contained in $\alpha(\hat{r})$. Hence, the evaluation of the matrix element $\langle IM | \Delta U | 00 \rangle$ reduces to the evaluation of $\langle IM | \alpha(\hat{r}) | 00 \rangle$. For a rotational model

$$\langle IM | \alpha(\hat{r}) | 00 \rangle = \frac{\delta_I}{(2I+1)^{1/2}} Y^*_{IM}(\hat{r}) , \tag{23}$$

where δ_I is the nuclear deformation. It is usual practice to rewrite δ_I as $\delta_I = \beta_I R$, where β_I is the deformation parameter and R is the radius of a given potential.

C. Spin-Dependent Interaction Potential

The form and strength of the spin-dependent perturbation potential, ΔU_{so}, has received considerable interest in the recent literature. The form we use in the theoretical calculations was proposed by Sherif and Blair[24]; it is called the full Thomas (FT) form. In this form the perturbation potential ΔU_{so} may be divided into two parts

$$\Delta U_{so} = U_{s,\rm def}(1) + U_{s,\rm def}(2) , \tag{24}$$

where

$$\Delta U_{s,\rm def}(1) = \left(\frac{\hbar}{m_\pi c}\right)^2 V_{so} \alpha(\hat{r}) \frac{1}{r} \frac{\partial}{\partial r} \frac{\partial f}{\partial R_{so}} \vec{\sigma} \cdot \vec{L} ,$$

$$\Delta U_{s,\rm def}(2) = \left(\frac{\hbar}{m_\pi c}\right)^2 V_{so} \frac{\partial f}{\partial R_{so}} \vec{\sigma} \cdot \left[\vec{\nabla}(\alpha_{so}(\hat{r})) \times \frac{1}{i} \vec{\nabla} \right] . \tag{25}$$

The first part is called the Oak Ridge (OR) form, since this is an unsymmetrized form of the interaction potential first used by an Oak Ridge group.[25] When both parts are used the interaction potential is called the full Thomas form. The computer program which was used to calculate the predictions was written by Sherif[23] and allows the use of either of the forms of ΔU_{so}.

D. DWBA Predictions

The predictions from the DWBA calculations labeled No def means that $\Delta U_{so} = 0$. The labels

OR and FT refer to the Oak Ridge and full Thomas forms of ΔU_{so}. Unless otherwise noted, $\beta_{so} = \beta_2$ where β_2 is the deformation of the central potential.

Included in the data which are compared with the theory are the elastic polarization and inelastic asymmetry data (see Fig. 7). The ^{58}Ni data were taken at 18.6 MeV. The ^{58}Ni elastic polarization data were reported by Kossanyi-Demay, de Swiniarski, and Glashausser.[26] The inelastic asymmetry data were reported by Glashausser, de Swiniarski, and Thirion.[27] The ^{54}Fe polarization and asymmetry data taken at 19.6 MeV have been reported by Escudié *et al.*[28] and Hendrie *et al.*[7] The theoretical predictions and the experimental results are compared in Figs. 1 through 7.

E. Discussion

The theoretical predictions are in general agreement with the experimental results for both nuclei. Note that there is, however, little difference between any of the forms for ΔU_{so} even when $\Delta U_{so} = 0$. This is not what one would normally expect, since quantities such as σ_1, S_1, C, the inelastic asymmetry, etc., are all spin-dependent quantities and would be expected to be strongly dependent on the strength of ΔU_{so}. This phenomenon has been pointed out by a number of authors,[5-7, 24, 25] Most of the strength for the spin-dependent interaction comes from the distorted waves which are solutions to the elastic scattering problem and, therefore, are the major contributions to the spin-dependent inelastic parameters.

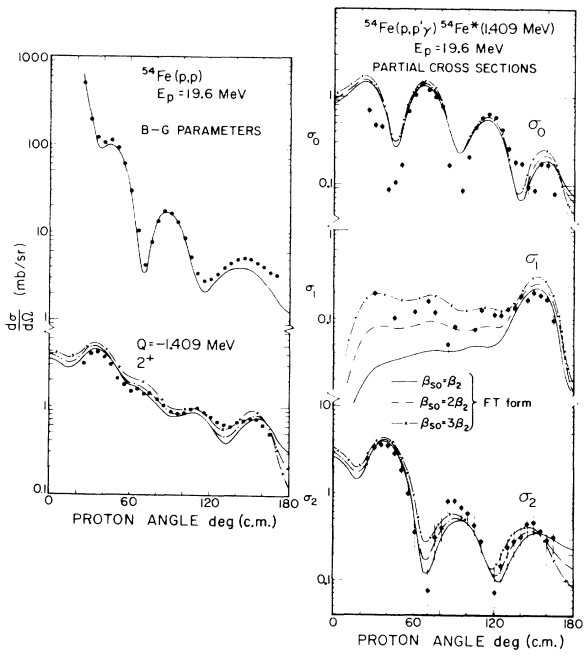

FIG. 8. Cross-section data for ^{54}Fe. The curves are DWBA predictions with the full Thomas form of ΔU_{so} and $\beta_{so} = \beta_2$, $2\beta_2$, and $3\beta_2$.

The insensitivity to the interaction potential makes it very difficult to determine anything about the form of ΔU_{so}. There is, however, evidence for preferring the FT form. There are some small improvements in the fits to σ_1, S_1, C, and the inelastic asymmetry as can be seen in the figures. More conclusive evidence comes from parameter A. Here a backward-angle peak is predicted *only* if the FT form is used as shown in Fig. 1. A further demonstration of the superiority of the FT form is given in Ref. 4. The predictions are not greatly changed by different choices of optical-model parameters.[29]

The FT form with $\beta_{so} = \beta_2$ improves the predictions for both the ^{54}Fe and ^{58}Ni data; however, the spin-dependent parameters for ^{58}Ni are fitted better than those of ^{54}Fe. In particular, the forward peak in the spin-flip probability S_1 for ^{54}Fe is not predicted, whereas S_1 for ^{58}Ni is well predicted. The prediction of σ_1 for ^{54}Fe is much too low at forward angles. There is also a marked difference in the inelastic asymmetry data at forward angles for these nuclei. The asymmetry difference has been pointed out for a number of even-even nuclei by Glashausser, de Swiniarski, and Thirion[27] at 18.6 MeV. The inelastic asymmetries for ^{54}Fe and ^{56}Fe at 19.6 MeV as reported by Escudié *et al.*[28] and Hendrie *et al.*[7] also show this difference between them. In one case, the asymmetry data for nuclei, such as ^{58}Ni and ^{56}Fe, are well predicted by the collective model; in the other case, asymmetry data for nuclei such as ^{54}Fe have the discrepancy at forward angles. This distinction can be seen in Fig. 7. The spin-flip probabilities of ^{54}Fe and ^{56}Fe have been measured by Hendrie *et al.*[7] in an attempt to resolve the difference; however, the spin-flip probabilities turned out to be very similar. An increase in β_{so} has been proposed by a number of authors to improve asymmetry predictions. Recently Raynal[30] has shown that with β_{so} equal to 2 or 3 times β_2, the ^{54}Fe asymmetry data at 18.6 MeV could be reasonably well matched. He bases the increase in β_{so} upon a microscopic description in cases where there is an open proton shell and a closed neutron shell, which is the case for ^{54}Fe.

Theoretical predictions are shown in Figs. 8 and 9 for the ^{54}Fe scattering data with the B-G parameters, the FT form, and $\beta_{so} = \beta_2$, $2\beta_2$, and $3\beta_2$. It is important to note that the increase in β_{so} does not necessarily imply a greater deformation of the spin-dependent potential; it is only a convenient means for increasing the strength of the spin-dependent force for exciting the state. A

review of the role of β_{so} has been given by Satchler.[31]

As can be seen from the figures, the increase in β_{so} greatly improves the predictions for many of the experimental quantities, in particular, those which depend on spin-flip amplitudes. The forward-angle asymmetry data are well fitted by $\beta_{so} = 2\beta_2$. The over-all fit to parameter A is improved by this increase. The forward-angle spin-flip probability and cross section are also improved. All of these improvements have been at forward angles – only in parameter C is there significant improvement in the fit at backward angles.

VI. CONCLUSION

The total inelastic cross section for each of the nuclei studied has been experimentally separated into substate cross sections. All of these cross sections, as well as the in-plane correlation parameters for both ^{54}Fe and ^{58}Ni, show good qualitative agreement with the collective-model theory.

Predictions for the isotropic term, parameter A, in the in-plane correlation function are very sensitive to the form of the spin-dependent perturbation potential, ΔU_{so}. The measurement of this term, therefore, clearly shows that the full Thomas form is superior for both ^{54}Fe and ^{58}Ni. The superiority of this form has been evident for inelastic asymmetry data at higher energies for some time but has not been conclusive at the lower energies used in these measurements.

An increase in the strength of ΔU_{so} is necessary in order to fit the asymmetry data for ^{54}Fe and represents the main difference between the interaction potentials for ^{54}Fe and ^{58}Ni. Thus, it appears that parameter A pins down the form of ΔU_{so}, while the inelastic asymmetry determines its strength.

The qualitative agreement of the collective-model predictions with the large amount of experimental data clearly demonstrates the validity of this model for the 2^+ states of ^{54}Fe and ^{58}Ni. The predictions, however, are not perfect. The details of the data will probably be better predicted if a more specific model is used and better calculational approximations are made.

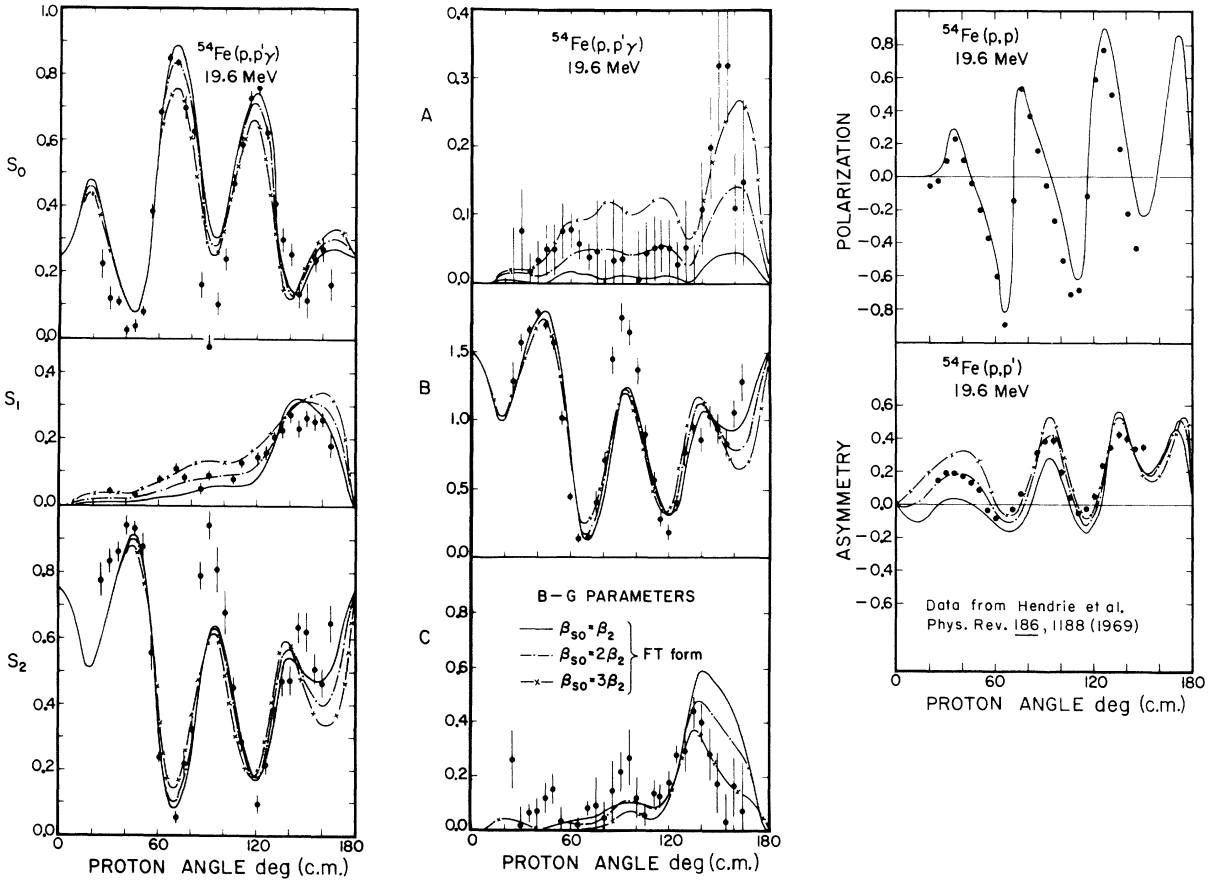

FIG. 9. Correlation and polarization data for ^{54}Fe. The curves are DWBA predictions with the full Thomas form of ΔU_{so} and $\beta_{so} = \beta_2$, $2\beta_2$, and $3\beta_2$.

The results from the ^{12}C measurements cannot be predicted by the collective model. However, comparison of the spin-dependent parameters of either ^{54}Fe or ^{58}Ni with those of ^{12}C gives evidence for using a different spin-dependent interaction for describing the ^{12}C results.

APPENDIX: SOLID-ANGLE CORRELATIONS

The solid-angle corrections take into account two effects. One is the finite geometry of the γ detector. These corrections are similar to those described in Ref. 1 and 6. The other is caused by the finite height of the proton detector. This causes $\hat{K}_f$ to vary, and since the z axis is determined by $\hat{K}_{\rm inc} \times \hat{K}_f$, the z axis is not well defined with respect to the γ detector. The proton detector effect is largest when the detector is near 0 or 180°.

The correction factors which occur in Eqs. (15) and (16) are derived by integrating the correlation function of Eq. (1),

$$\overline{W} = \mathrm{Tr}\rho \frac{\int \eta d\Omega_\gamma d\phi_p}{\int d\Omega_\gamma d\phi_p} . \tag{26}$$

The density matrix ρ is assumed not to be a function of θ_p.

Substate interference terms from Eq. (25) that do not occur in the point detector geometry correlation functions, Eqs. (5) and (10), have been neglected in the corrections. The magnitudes of these neglected terms cannot be directly evaluated, since they contain elements of ρ which have not been determined.

TABLE II. Examples of solid-angle correction factors.

ϕ_p (deg)	$\bar{A}$	$\bar{B}$	$\bar{C}$	C_1	C_2	$\bar{D}$	$\bar{G}$	$\bar{F}$
170	0.91	0.05	0.0005	0.91	0.94	0.10	0.92	0.03
90	0.98	0.01	0.00	0.98	0.97	0.06	0.95	0.02

Worst-case values ($\phi_p = 170°$) for the correction factors and best-case values ($\phi_p = 90°$) are shown in Table II. A complete derivation of the correction factors is given in Ref. 29.

ACKNOWLEDGMENTS

We are deeply indebted to Donald M. Patterson, Jüri Eenmaa, Thomas K. Lewellen, and Phyllis A. Russo for help with the data collection; to Dr. W. G. Weitkamp, J. W. Orth, Mrs. G. Rohrbaugh, and other members of the University of Washington Nuclear Physics Laboratory staff for efficient operation of the three-stage tandem accelerator and help with many of the experimental details; to Mrs. H. Turner and Mrs. P. Douglas for assistance in the preparation of this manuscript.

We wish to especially thank Professor J. S. Blair for his numerous discussions and suggestions, and Dr. H. Sherif for the use of his computer program.

†Work supported in part by the U. S. Atomic Energy Commission.

*This work was submitted by one of us (J. R. T.) in partial fulfillment of the requirements for the Ph. D. degree at the University of Washington.

‡ Present address: Department of Physics, Purdue University, Lafayette, Indiana 47907.

[1]F. H. Schmidt, R. E. Brown, J. B. Gerhart, and W. A. Kolasinski, Nucl. Phys. 52, 353 (1964).

[2]This energy matches that of the asymmetry measurements performed at Saclay.

[3]J. R. Tesmer, J. Eenmaa, T. Lewellen, D. M. Patterson, and F. H. Schmidt, Bull. Am. Phys. Soc. 14, 1220 (1969); J. R. Tesmer, J. Eenmaa, T. Lewellen, D. M. Patterson, P. A. Russo, and F. H. Schmidt, *ibid.* 15, 1680 (1970).

[4]J. R. Tesmer and F. H. Schmidt, Phys. Rev. Letters 26, 857 (1971).

[5]J. Eenmaa, F. H. Schmidt, and J. R. Tesmer, Phys. Letters 28B, 321 (1968).

[6]W. A. Kolasinski, J. Eenmaa, F. H. Schmidt, H. Sherif, and J. R. Tesmer, Phys. Rev. 180, 1006 (1969).

[7]D. L. Hendrie, G. Glashausser, J. M. Moss, and J. Thirion, Phys. Rev. 186, 1188 (1969).

[8]L. C. Biedenharn and M. E. Rose, Rev. Mod. Phys. 25, 729 (1953).

[9]S. Devons and J. B. Goldfarb, in *Encyclopedia of Physics*, edited by S. Flugge (Springer, Berlin, 1957), Vol. 42.

[10]A. Bohr, Nucl. Phys. 10, 486 (1959).

[11]Provided by a National Science Foundation grant.

[12]T. D. Hayward, Ph.D. thesis, University of Washington, 1969 (unpublished).

[13]A. C. G. Mitchell, in *Beta- and Gamma-Ray Spectroscopy*, edited by K. Siegbahn (Interscience, New York, 1955).

[14]I. S. Sherman, R. G. Roddick, and A. V. Metz, IEEE Trans. Nucl. Sci. 3, 500 (1968).

[15]D. M. Patterson, Nuclear Physics Laboratory Annual Report, University of Washington, 1970 (unpublished), p. 45.

[16]T. D. Hayward and F. H. Schmidt, Phys. Rev. C 1, 923 (1970).

[17]A. J. Ferguson, *Angular Correlation Methods in Gamma-Ray Spectroscopy* (Wiley, New York, 1965).

[18]J. S. Blair, Phys. Rev. 115, 928 (1959).

[19]This meaning of adiabatic is in contradiction to the meaning as applied, for example, to the classical adiabatic expansion of a gas.

[20]J. S. Blair and L. Wilets, Phys. Rev. 121, 1493 (1961).

[21]H. Sherif, Can. J. Phys. 49, 983 (1971).
[22]F. D. Becchetti, Jr., and G. W. Greenlees, Phys. Rev. 182, 1190 (1969).
[23]H. Sherif, Ph.D. thesis, University of Washington, 1968 (unpublished).
[24]H. Sherif and J. S. Blair, Phys. Letters 26B, 489 (1968).
[25]M. P. Fricke, R. M. Drisko, R. H. Bassel, E. E. Gross, B. V. Morton, and A. Zucker, Phys. Rev. Letters 16, 746 (1966).
[26]P. Kossanyi-Demay, R. de Swiniarski, and C. Glashausser, Nucl. Phys. A94, 513 (1967).
[27]C. Glashausser, R. de Swiniarski, and J. Thirion, Phys. Rev. 164, 1437 (1967).
[28]J. L. Escudié, J. C. Faivre, W. Haeberli, B. Mayer, and N. Poutcherov, Centre à l'Energie Atomique, Department de Physique Nucleaire, Compte Rendu d'Activité (unpublished).
[29]J. R. Tesmer, Ph.D. thesis, University of Washington, 1971 (unpublished).
[30]J. Raynal in *Proceedings of the Third International Symposium on Polarization Phenomena in Nuclear Reactions, Madison, 1970,* edited by H. H. Barschall and W. Haeberli (University of Wisconsin Press, Madison, Wisc., 1971).
[31]G. R. Satchler, in *Proceedings of the Third International Symposium on Polarization Phenomena in Nuclear Reactions* (see Ref. 30).

PHYSICAL REVIEW C VOLUME 5, NUMBER 3 MARCH 1972

Electromagnetic Transitions in V^{51} and Mn^{53}†

A. S. Goodman and D. J. Donahue
Department of Physics, University of Arizona, Tucson, Arizona 85721
(Received 7 October 1971)

Attenuated Doppler shifts and particle–γ-ray angular correlations have been measured and interpreted to yield properties of electromagnetic transitions in V^{51} and Mn^{53}. Mean lives have been obtained for states at 1.609, 1.813, 2.402, 2.670, and 2.699 MeV in V^{51}, and for states at 1.288, 1.440, 1.619, 2.277, 2.406, 2.575, 2.641, and 2.705 MeV in Mn^{53}. Possible multipole mixing ratios have been deduced for the transitions (energies in MeV) $0.378 \rightarrow 0$, $1.288 \rightarrow 0.378$, $1.619 \rightarrow 0$, $2.277 \rightarrow 0$, and $2.406 \rightarrow 1.288$ in Mn^{53}. A possible identification of a $\frac{15}{2}^-$ state in Mn^{53} is presented. From these results and the results of other workers, transition probabilities in V^{51} and Mn^{53} have been calculated and compared (i) with one another, (ii) with a $(1f_{7/2})^n$ pure-configuration shell-model calculation, and (iii) with a mixed-configuration calculation.

I. INTRODUCTION

In a simple shell-model picture, the nuclei $_{23}V^{51}$ and $_{25}Mn^{53}$ can be considered to contain a closed shell of 28 neutrons and, respectively, three protons and three proton holes in the $1f_{7/2}$ shell. There are several predictions of the pure-configuration shell-model calculation[1] which make an investigation of the electromagnetic transitions among states of these nuclei of interest. First, since all electromagnetic transitions among $(1f_{7/2})^n$ states would be between states of the same j shell, the pure-configuration model predicts that all dipole transitions are strictly forbidden. Second, since the model treats particles and holes equivalently, transition probabilities in the two nuclei should be identical. Third, calculations have recently been made[2] which indicate that many $E2$ transition probabilities in the $1f_{7/2}$ shell can be predicted with a single assumption concerning the effective charge of the neutrons and protons in this shell. Finally, in addition to the pure-configuration calculations, mean lives of states in Mn^{53} have recently been obtained from calculations[3] which include contributions from single-particle levels other than the $1f_{7/2}$ shell.

In the work presented here, some electromagnetic transition probabilities for the two nuclei have been measured and compared with predictions using both the simple and the more complicated model. We have used the reactions $Ti^{48}(\alpha, p\gamma)V^{51}$ and $Cr^{50}(\alpha, p\gamma)Mn^{53}$ to study the level structure and mean lives for states up to 2.7 MeV in V^{51}, and the level structure, decay scheme, lifetimes, multipole mixing ratios, and branching ratios, where possible, for states up to 2.705 MeV in Mn^{53}. Mean-life measurements in both cases were made using a p-γ coincidence version of the Doppler-shift-attenuation method.[4] Multipole mixing ratios in Mn^{53} were determined by observing the angular correlations between protons from the reaction $Cr^{50}(\alpha, p\gamma)Mn^{53}$ and the emitted γ rays. This technique is described by Litherland and Ferguson as method II.[5]